Available online at www.sciencedirect.com
ScienceDirect
Trans. Nonferrous Met. Soc. China 32(2022) 1169−1177
Transactions of Nonferrous Metals Society of China
www.tnmsc.cn

High-strength Ti−BN composites with core-shell structured matrix and network-woven structured TiB nanowires

Li-qing HUANG[1], Qun HUANG[2]

1. School of Mechanical and Mining Engineering, The University of Queensland, Brisbane, QLD 4072, Australia;
2. State Key Laboratory of Powder Metallurgy, Central South University, Changsha 410083, China

Received 13 April 2021; accepted 26 November 2021

Abstract: A novel architectural Ti composite composed of network-woven structured TiB nanowires in a core-shell structured Ti matrix was fabricated to improve the strength of Ti matrix composites (TMCs), where the shell consists of rich N solute atoms while the core is deficient of N solute atoms through spark plasma sintering of powder mixtures of Ti powder and BN nano-powder. The phase composition, morphology, element distribution, and mechanical properties of prepared samples were analyzed by X-ray diffraction (XRD), scanning electron microscope (SEM), electron probe microanalyzer (EPMA), and electronic universal material testing machine. The results indicate that the TMCs with designed architectures have been successfully achieved, and the as-prepared Ti−2BN (wt.%) composite exhibits an ultimate compressive strength of ~1.8 GPa with a strain-to-fracture of ~9%, while the Ti−1BN (wt.%) attains an ultimate compressive strength of ~1.6 GPa and a strain-to-fracture of ~20%. Moreover, the roles of the hybrid reinforcement structures in strengthening the Ti composites were discussed.
Key words: titanium matrix composites; TiB nanowires; nitrogen; network-woven structure; core-shell structure

1 Introduction

Titanium matrix composites (TMCs) can achieve the desired balance among strength, toughness, modulus, ductility and high-temperature durability, making them attractive for advanced structural materials applications [1−6]. The TiB whiskers have been regarded as the most promising reinforcements for the Ti matrix because of their high modulus, similar coefficient of thermal expansion to that of the Ti matrix, and negligible solubility in the Ti matrix [3,4]. However, the TiB whiskers formed in the Ti matrix are usually up to a few microns in diameter with low aspect ratios (2−5 μm in diameter and 10−20 μm in length), thus imparting limited strengthening effect on the matrix [3,7].

Recently, KOO et al [8] have fabricated the TiB nanowires reinforced TMCs and reported the strengthening effect by the TiB nanowires. Mechanical alloying (MA) was employed to homogeneously disperse submicron TiB_2 powder (<500 nm) into the Ti alloy powder. The powder mixture was then consolidated by spark plasma sintering (SPS) to allow the in-situ formation of TiB nanowires in the Ti matrix via reactions between Ti and TiB_2. More recently, we fabricated high tensile-strength and ductile Ti6Al4V composites reinforced by TiB nanowires with a network-woven structure [9]. A key step of producing this unique Ti−TiB structure is the use of a low-energy ball milling process by which boron (B) or boron carbide (B_4C) nano-powder particles (<100 nm) were attached to the surface of the Ti powder particles. The as-fabricated TMCs achieved both high strength arising from the TiB nanowires and good ductility due to the architectural structure.

Corresponding author: Qun HUANG, Tel: +86-731-88836513, E-mail: huangqun@csu.edu.cn
DOI: 10.1016/S1003-6326(22)65864-3

TiB_2 and B_4C are commonly used as the B source for the in-situ formation of TiB whiskers in a Ti matrix [1,2,10,11]. Another option is boron nitride (BN) which can supply B as well as the N source. N has a high solubility in Ti and possesses a potent solid-solution strengthening effect [12,13]. For example, ZHANG et al [14,15] have produced high-strength core-shell-structured Ti−N alloys featured with soft Ti cores and hard Ti−N solid-solution shells. These alloys were prepared by SPS of N-pre alloyed Ti powders, where N was introduced into the outer layers of the Ti powder particles by gas nitriding. As previously mentioned, BN can also be considered as a source of N for the fabrication of Ti−N alloys. However, up till now, BN has been mainly used in preparing TiB−TiN ceramics [16−20]. In a recent study [21], we fabricated high tensile strength and ductile Ti−Fe−N−B alloys through the addition of a small amount of BN (≤0.50 wt.%). The amount of the introduced N was insufficient to lead to the formation of the core-shell structures reported in Refs. [13,14]. Consequently, the resultant TiB nanowires played a primary strengthening role.

In this work, the high-content additions of BN nano-powders were used as both sources of B and N for the fabrication of TMCs, achieving a hybrid reinforcement structure that consists of both a network-woven structured TiB and a core-shell structured matrix. Moreover, the low-energy ball milling mixing method used in this study was also compared with the traditional mixing (powder blending), showing its effectiveness in deagglomerating of nano-powder particles for the fabrication of fully dense composites. Meanwhile, the microstructures and mechanical properties of the as-sintered TMCs samples were characterized and discussed.

2 Experimental

Gas atomized spherical Ti powder (0−45 μm, ~18 μm in average, 0.14 wt.% O, 0.02 wt.% N, AP&C Inc., Canada) and nanosized BN powder (hexagonal phase, 99.9%, ~50 nm, DK Nano Inc., China) were used to prepare Ti−xBN (x=0, 0.5, 1, and 2 wt.%) powder mixtures. The powders were ball-milled in a steel jar with a ball-to-powder ratio of 2:1 under an argon atmosphere for 3 h using a Turbula Mixer at a mixing speed of 150 r/min. The resultant powder mixture was loaded into a graphite die which had an inner diameter of 20 mm, and then heated to 1000 °C at 60 °C/min and sintered at 1000 °C for 7 min under a pressure of 30 MPa. The sintering was conducted by SPS (Fuji SPS211Lx, pulsed current equipped). The as-sintered samples were ground and polished, and selected samples were deeply etched with a mixed solution of purified water, nitric acid, and hydrofluoric acid at a mole ratio of 85:10:4. The phase constituents were identified using a Bruker AXS X-ray diffractometer (XRD). Microstructures were characterized using SEM (JEOL JSM 7001F). Elemental distribution (N, B, Ti) was analyzed by a JEOL JXA−8230 electron probe microanalyzer (EPMA) equipped with wavelength-dispersive spectroscopy (WDS). And the accelerating voltage for EPMA is within the range of 1−30 kV, the probe current is in the range of 10^{-12}−10^{-15} A, and the detectable wavelength range of X-ray is 0.087−9.3 nm. The overall O and N contents in each sample were determined using a TCH−600 H/N/O analyzer. Compression tests were performed on an Instron−5584 with a strain rate of 1×10^{-3} s^{-1} using cylindrical specimens (d3.5 mm × 7 mm) with an infrared extensometer.

3 Results and discussion

3.1 Powder mixing

Figure 1 shows the morphology of Ti powder particles before and after the low-energy ball milling with 1 wt.% BN nanoparticles. The initial Ti powder particles possessed a spherical morphology (Fig. 1(a)) with an average diameter of ~18 μm. Figure 1(b) shows an enlarged view of a region marked on the surface of a Ti particle in Fig. 1(a), showing that the surface was clean and smooth. After low-energy ball milling, the Ti powder particles remained nearly spherical but the surfaces were no longer smooth (Fig. 1(c)). A region selected from the surface of a Ti particle (marked with a rectangle in Fig. 1(c)) is shown in Fig. 1(d). BN nanoparticles were uniformly coated onto the surface of the Ti particle.

Nanoparticles are prone to aggregate together due to the inter-nanoparticle forces [22]. The big clustered BN powders are obvious in traditional mixing processes. Compared with traditional mixing processes, the low-energy ball milling process was conducted with the assist of steel balls.

The collision between steel balls and powders during processing greatly hinders the clustering of BN nanoparticles, leading to the homogenous and tight coating of BN nano-particles on the surfaces of Ti powder particles. In order to reveal the significance of the low-energy ball milling process, two kinds of Ti−2BN composites were prepared through the same sintering procedure, one using the as-milled powder mixture and the other using the as-mixed powder mixture. Figure 2 shows SEM images of the two kinds of Ti−2BN samples prepared with different powder mixtures.

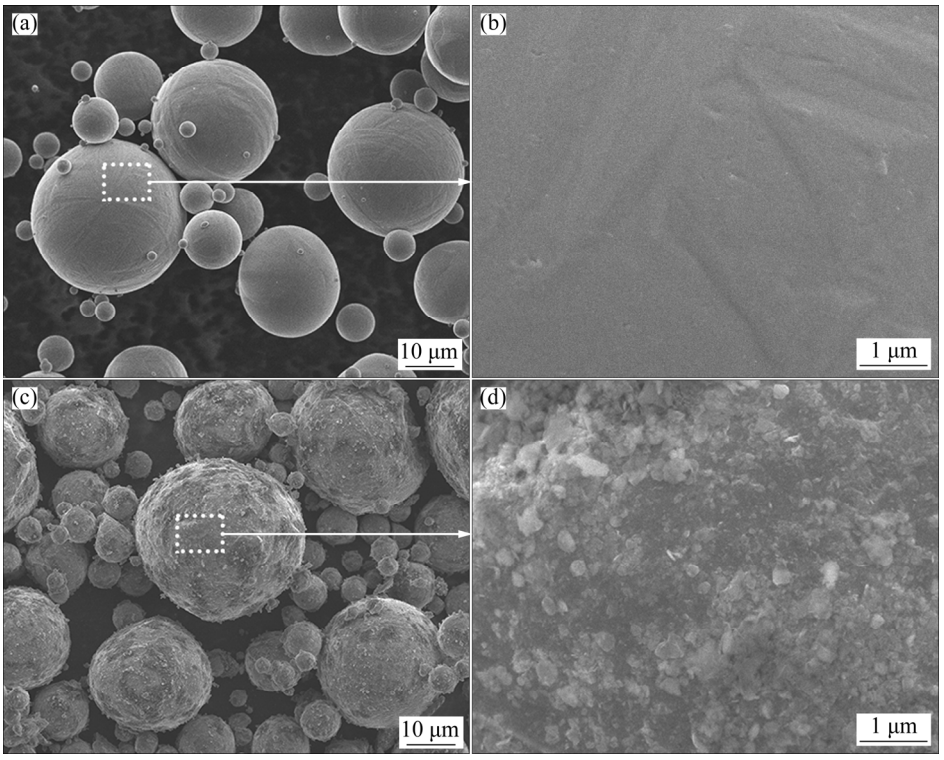

Fig. 1 Morphologies of as-received Ti powder particles (a, b) and ball-milled Ti−1BN powder mixtures (c, d)

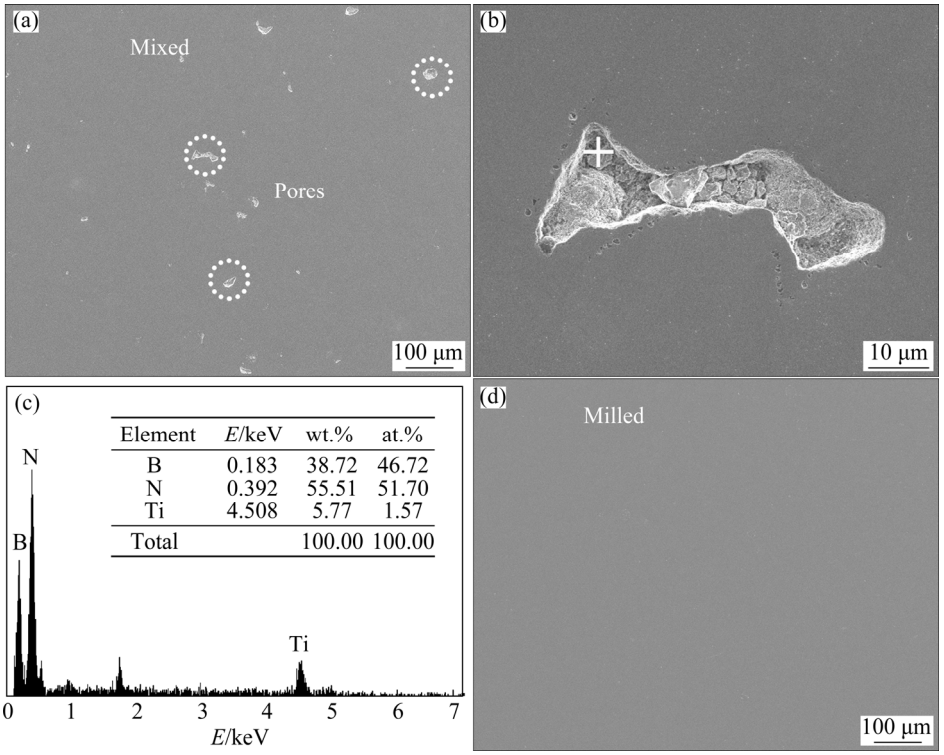

Element	*E*/keV	wt.%	at.%
B	0.183	38.72	46.72
N	0.392	55.51	51.70
Ti	4.508	5.77	1.57
Total		100.00	100.00

Fig. 2 SEM images of as-sintered Ti−2BN samples prepared by traditional mixed (a, b, c) and low-energy ball-milled (d) powder mixtures ((c) is an EDS result obtained from point "+" shown in (b))

The sample sintered from as-mixed powder mixture (Fig. 2(a)) reveals a considerable number of large pores on the polished surface (up to tens of microns, marked as white circles for example), and one of them was zoomed to be shown in Fig. 2(b). EDS analyses revealed that both B and N elements were concentrated around the pores, and even unreacted BN particles existed (Fig. 2(c)). However, the sample (Fig. 2(d)) sintered from the as-milled powder mixture showed no visible pores. Nanoparticles are prone to aggregate together due to the complex and varied inter-nanoparticle forces [22]. The traditional mixing process was incapable of de-agglomerating BN nanoparticles clusters, so pores formed in regions with excessive amounts of BN nano-particles during the sintering process. Nonetheless, with the help of mechanical energy provided by the steel balls, the mechanical milling process obviated the abovementioned unfavorable outcome. Conclusively, the low-energy ball milling is an effective and necessary method for uniformly dispersing BN nanoparticles onto surface of Ti powder particles and for preparing the pore-free TMCs by the sintering.

3.2 Phase identification and microstructural characterization

As the composite made from the as-mixed powder mixture is just for comparison shown above, all composites described below are the composites made from the as-milled powder mixtures if not otherwise specified. Table 1 lists the O and N contents in the as-sintered Ti−*x*BN (*x*=0−2 wt.%) composites. Compared with commercially pure (CP) Ti samples, Ti−BN samples made from ball-milled powder mixtures showed a higher oxygen content. The measured N contents in all Ti−BN samples agreed well with their theoretical compositions. For example, the addition of 2 wt.% BN corresponded to the introduction of 0.87 wt.% B and 1.13 wt.% N theoretically, and the N content in the as-sintered Ti−2BN composites was measured to be 1.11 wt.%. The volume fraction of the TiB nanowires in the Ti−2BN composite was calculated to be 4.7%. Figure 3 exhibits the XRD data obtained from the as-sintered Ti−BN samples (made from the as-milled powder mixtures, the same for all the samples mentioned below). Both *α*-Ti and TiB phases were detected but no titanium nitride phase

Table 1 Measured O and N contents in as-sintered Ti−*x*BN composites (wt.%)

Sample	O	N
Ti	0.10	0.01
Ti−0.5BN	0.14	0.28
Ti−1BN	0.18	0.53
Ti−2BN	0.18	1.11

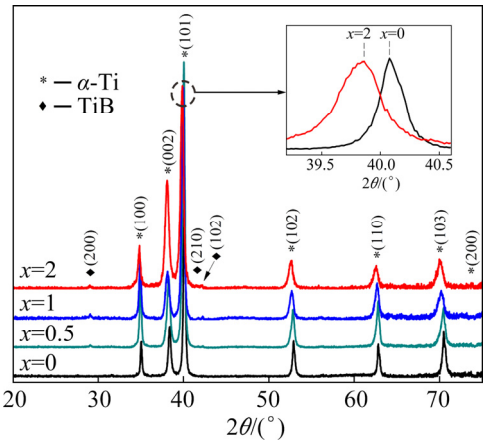

Fig. 3 XRD patterns for as-sintered Ti−*x*BN (*x*=0, 0.5, 1, 2) composites

was observed. During SPS at 1000 °C, BN particles react with Ti particles to form TiB and N solutes [23]. Since N has significant solubility in Ti at elevated temperatures (~8 wt.% at 1000 °C) while the cooling rate after SPS is high [24], the N atoms are expected to be in the Ti matrix as solutes. ZHANG et al [15] also reported that no titanium nitrides were detected in the SPS- processed Ti−0.95N (wt.%) alloy. The dissolved N atoms caused lattice expansion of the *α*-Ti phases, leading to a shift of the XRD peaks for *α*-Ti to lower 2θ values (θ is the diffraction angle), while the positions of the TiB peaks were not affected. As shown in the inset in Fig. 3, the 2θ value for the (101) plane of the *α*-Ti phase in the pure Ti sample is 40.08°, while it was shifted to 39.85° in the Ti−2BN composite. The decrease in the 2θ diffraction angle corresponds to an expansion in the adjacent lattice planes of ~0.189% ($d_2/d_1=\sin\theta_1/\sin\theta_2$). Given that the lattice parameters of Ti vary with O and N contents [13], the expansion ratio can be roughly calculated to be 0.178% when the O and N contents were increased from 0.1 and 0.01 (wt.%) to 0.18 and 1.11 (wt.%), respectively. It agrees well with the experimental result of this work.

The microstructures of the Ti−2BN composite were characterized by SEM and EPMA mapping, and the results are shown in Fig. 4. Figure 4(a) shows a secondary electron (SE) image of the as-polished Ti−2BN composite. Figure 4(b) shows the SEM image of the Ti−2BN composite after deep etching, which shows TiB nanowires with dimensions of 10−30 μm in length and 50−200 nm in diameter. The TiB nanowires distributed inhomogeneously, forming a three-dimensional network-woven architecture. This structure had been previously reported in the TMCs using B or B_4C nano-powder as raw materials [7,23]. The TiB nanowires nucleated on the surfaces of the Ti powder particles coated with BN nanoparticles, and then grew into nearby Ti matrix grains along certain directions related to the Ti/TiB orientation relationship, eventually forming a network-woven architecture. A similar structure was observed in the Ti−0.5BN and Ti−1BN composites fabricated in this study. When micro-sized B precursors (>1 μm) were used, a similar network structure of TiB was formed in the Ti matrix, while the TiB phase was in the form of micro-sized whiskers (several microns in diameter) [10,25].

Figure 4(c) shows a backscattered electron (BSE) image of the Ti−2BN composite. The dark−bright contrast indicates an inhomogeneous distribution of the elements, where darker regions are enriched in lighter elements. The EPMA maps shown in Figs. 4(d−f) display the distribution of Ti, B, and N. The significant amount of B introduced to this alloy is shown as a network structure in Fig. 4(e), which is consistent with the distribution of TiB in Fig. 4(b). Moreover, the distribution of N led to the formation of a core-shell structure as indicated in Figs. 4(c) and (f). The shell was identified to be the outer layer of a Ti powder particle that is enriched with N, while the core is the inner part of the particle that is deficient of N.

When heated up to the isothermal sintering temperature, BN nanoparticles started to react with Ti powder particles to form TiB nanowires and release N atoms. The N would be concentrated in the outer region of the Ti powder particles due to insufficient diffusion. N increases the transition temperature from α-Ti phase to β-Ti phase. According to the Ti−N phase diagram [24], at 1000 °C, α-Ti phase containing less than ~0.35 wt.% N will transform to β-Ti phase, while

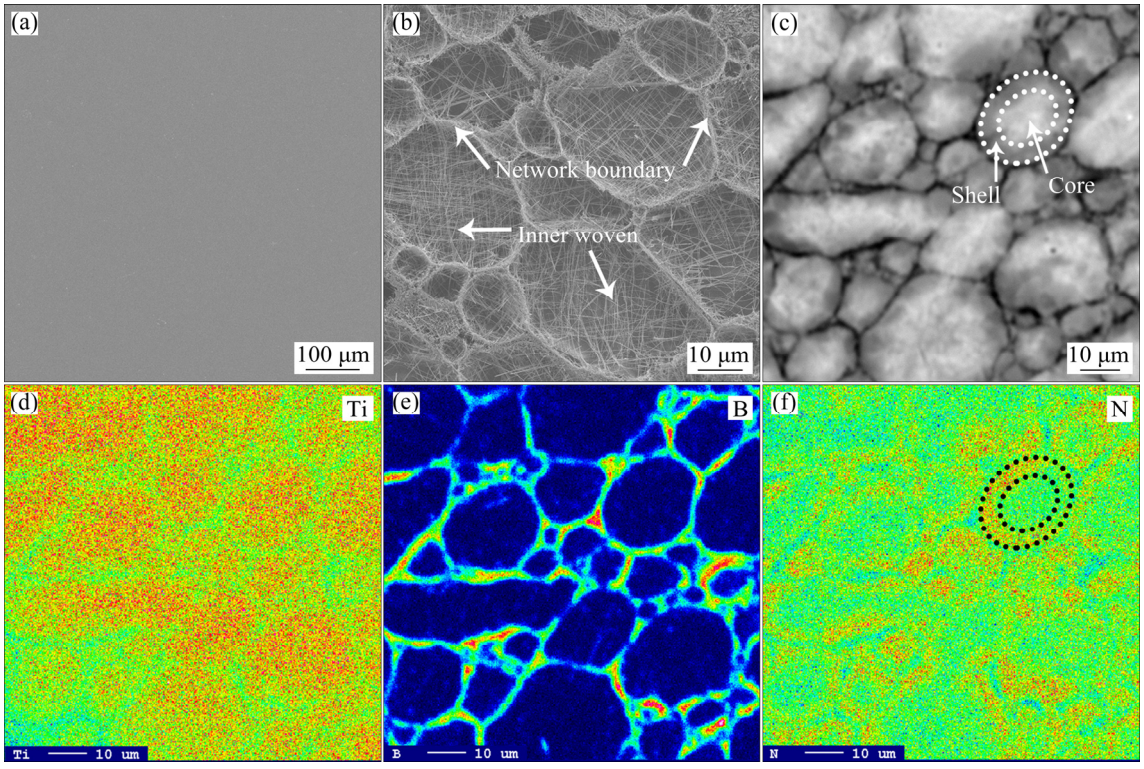

Fig. 4 SEM images of Ti−2BN composite: (a) SE image after polishing; (b) SE image after deep etching; (c) BSE image after polishing; (d−f) EPMA-WDS mapping images for Ti, B, and N in region (c) (The blue color represents low content, while the red means high content)

that containing more than ~0.73 wt.% N can remain to be α-Ti phase. Therefore, during the sintering of Ti−2BN at 1000 °C, the outer layers of a Ti particle were kept in the α-Ti phase state even though the inner region transformed to β-Ti phase. N atoms have a much slower diffusion rate and higher solubility in the α-Ti phase than those in the β-Ti phase [26]. As a result, the outer shell became enriched with N. The core-shell structure was reported that Ti−N alloys were sintered from surface nitrided Ti powders by SPS [14,15]. In brief, owing to the growth of TiB, the diffusion of N atoms, and the influence of N on the temperature of the transformation from α phase to β phase, a hybrid reinforcement structure was formed in the Ti matrix. The core-shell structure faded slightly in the Ti−1BN composite and was essentially absent in the Ti−0.5BN composite because of the limited N content. Compared with the traditional gas nitriding process, the use of BN nanopowders is a simpler and more efficient method of N supply, which is expected to be applied in other alloys and composite systems.

3.3 Mechanical performance

Figure 5 shows the representative compressive true strain−stress curves of the as-sintered Ti−BN composites. For comparison, the ultimate compressive true strength and true strain values of the core-shell structured Ti−0.44N, Ti−0.95N and Ti−1.45N alloys reported in Ref. [13] are also presented. Detailed values of the yield strength

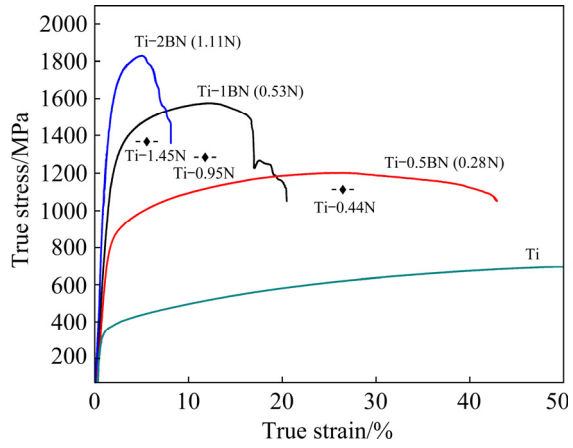

Fig. 5 Compressive true strain−true stress curves of as-sintered Ti−BN composites (measured N contents are shown in brackets, wt.%) and comparison with recently reported core-shell structured Ti−1.45N, Ti−0.44N and Ti−0.95N (wt.%) alloys [13]

($\sigma_{0.2}$), ultimate compressive strength (σ_b), and fracture strain of the Ti−BN composites are summarized in Table 2. The compressive strength of the composites increased with increasing BN content while the fracture strain decreased. The Ti−2BN composite achieved an ultimate compressive strength of ~1.8 GPa with the fracture strain of 9.2%. As shown in Fig. 5, both the Ti−2BN and Ti−1BN composites exhibit superior mechanical performance to the previously reported core-shell structured Ti−N alloys [13].

Table 2 Compression test results of as-sintered Ti−xBN composites

Sample	$\sigma_{0.2}$/MPa	σ_b/MPa	Strain/%
Ti	318±6	–	–
Ti−0.5BN	718±11	1205±13	44.6 ±2.7
Ti−1BN	1207±15	1641±20	20.2±2.4
Ti−2BN	1340±20	1835±21	9.2±0.7

The Ti−BN composites fabricated in this study are strengthened by both network-woven structured TiB nanowires and N solute atoms in the abovementioned shells or surface layers of each matrix grain. An inhomogeneous distribution of reinforcements such as hard phases encapsulating soft phases has been reported to be beneficial to the overall strengthening effect [27]. TiB nanowires with a 3D network-woven structure have proved to be capable of offering a high strengthening effect while retaining good ductility of Ti matrix [9]. The reduction in ductility from Ti−1BN to Ti−2BN could mainly be attributed to the increased N content [11]. As shown in Fig. 5, the strain−stress curves for the Ti−1BN and Ti−2BN composites became zigzagged after reaching the maximum compressive strength during compression. This phenomenon, i.e., a sudden reduction in stress without an overall sudden rupture, indicates that the composites undergo a torturous fracture process.

Figure 6 shows representative fracture surfaces of the Ti−1BN and Ti−2BN composites after the compression test. A torturous fracture surface of the Ti−1BN is shown in Fig. 6(a), which exhibits large areas of fine-scaled torturous fracture morphology together with micro-sized dimples, inner cracks, and small cleavage facets. Figure 6(b) reveals that the fine torturous fracture morphology mainly results from the fracture of TiB nanowires and their

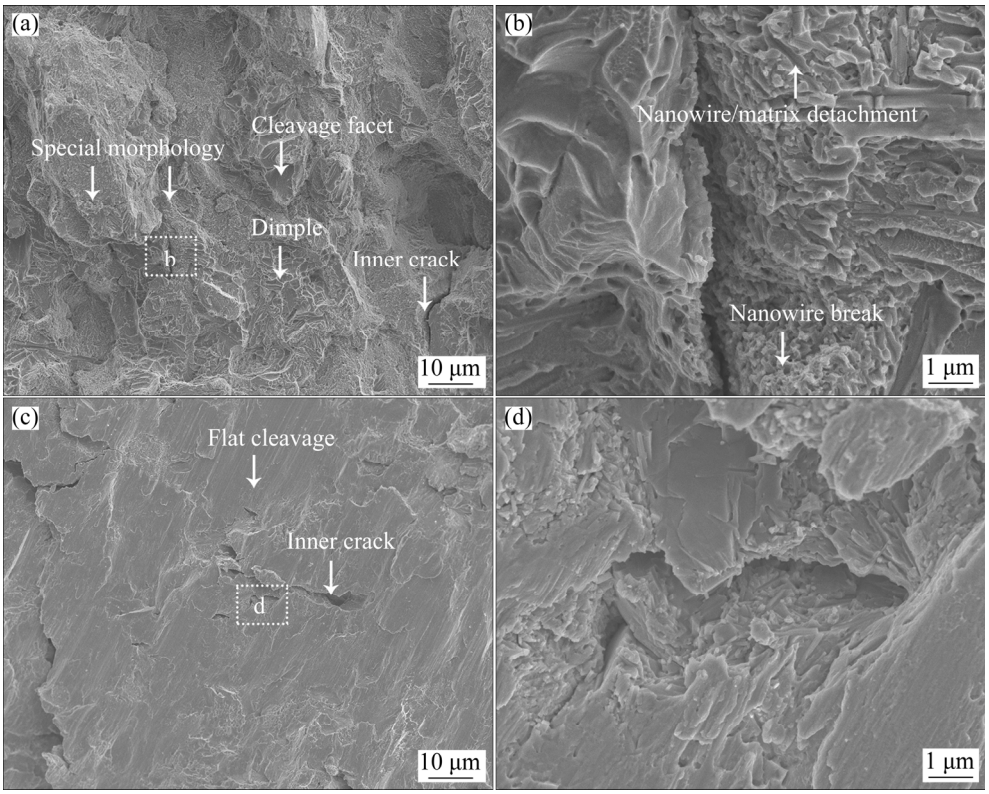

Fig. 6 Representative compression fracture surface characteristics of Ti−1BN (a, b) and Ti−2BN (c, d) composites

detachment from the matrix. During compression, load transfer occurs from the Ti matrix to the TiB nanowires. The stress will be concentrated in the TiB network boundary regions, where a significant number of TiB nanowires exist, thus leading to the fracture of nanowires or interfacial detachment between the nanowires and the matrix [28,29]. The ultrafine torturous fracture morphology shown in Fig. 6(b) is caused by the breakage of the TiB nanowires, while the channel-shape structure is assumed to be associated with the detachment between the nanowires and the matrix. Therefore, the regions were correspondingly marked as nanowire break and nanowire/matrix detachment in Fig. 6(b). Owing to the 3D distribution of the woven TiB nanowires, cracks can be deflected and also branched to form secondary cracks at junctions of the network during propagation. The preferred paths for crack propagation and branching were observed to be along the network boundaries (Fig. 6(b)), which is consistent with the tensile fracture surface characteristics observed for TiB nanowires reinforced Ti6Al4V composites [9]. Crack deflection and branching caused by the presence of second phase can significantly enhance the damage tolerance of the material [25,30,31]. As shown in Fig. 6(c), large cleavage facets are observed in the Ti−2BN composites due to the presence of both TiB nanowires and N atoms in the Ti matrix. Because of the existence of the network-woven architecture of TiB nanowires, crack deflection or branching (as shown in Figs. 6(c) and (d)) can be regarded as the primary reason for the formation of the zigzag-shaped strain−stress curves shown in Fig. 5. In addition, high-aspect-ratio nanowire-like ceramics can be bent to a greater extent than other forms of ceramics without abrupt fracture, or they can even exhibit limited plasticity, which could be expected to aid the achievement of desirable ductility for the TMCs concerned [32,33].

4 Conclusions

(1) The ball milling process helped to avoid clustering of the BN nanoparticles and consequently to coat the BN nanoparticles homogenously and firmly onto the Ti powder particle surfaces. After the reaction between NB and Ti at high temperatures, the newly formed TiB nanowires were developed into a network-woven structure, while the N solute atoms were mainly

distributed in the outer layers of each Ti powder particle to form a core-shell structure, and all Ti−BN composite showed a pore-free microstructure.

(2) The Ti−BN composites were strengthened by TiB nanowires with a network-woven structure and the N solute atoms in solid solution. And the strength of the Ti−BN composites increased with increasing BN content. The Ti−2BN composite reached an ultimate compressive strength of ~1.8 GPa with a fracture strain of ~9.2%. In Ti−1BN and Ti−2BN composites, crack deflection and crack branching were observed near the network-woven architecture of TiB during crack propagation, which contributed to the high toughness and damage tolerance of the TMCs.

Acknowledgments

This work was supported by the Australian Research Council (No. LP130100913) and by the Baosteel-Australia Joint Research and Development Centre on the Project (No. BA110014LP). Li-qing HUANG thanks the China Scholarship Council for providing his PhD stipend. The Australian Microscopy & Microanalysis Research Facility at the University of Queensland was acknowledged for accessing microscopic facilities.

References

[1] TJONG S C, MAI Y W. Processing-structure-property aspects of particulate- and whisker-reinforced titanium matrix composites [J]. Composites Science and Technology, 2008, 68(3/4): 583−601.

[2] MORSI K, PATEL V V. Processing and properties of titanium–titanium boride (TiB_w) matrix composites — A review [J]. Journal of Materials Science, 2007, 42(6): 2037−2047.

[3] SAITO T. A cost-effective P/M titanium matrix composite for automobile use [J]. Advanced Performance Materials, 1995, 2(2): 121−144.

[4] IBRAHIM I A, MOHAMED F A, LAVERNIA E J. Particulate reinforced metal matrix composites—A review [J]. Journal of Materials Science, 1991, 26(5): 1137−1156.

[5] LIN Ying-hua, LIN Zhen-heng, CHEN Qing-tang, LEI Yong-ping, FU Han-guang. Laser in-situ synthesis of titanium matrix composite coating with TiB–Ti network-like structure reinforcement [J]. Transactions of Nonferrous Metals Society of China, 2019, 29(8): 1665−1676.

[6] GOGHERI M S, KASIRI-ASGARANI M, BAKHSHESHI-RAD H R, GHAYOUR H, RAFIEI M. Mechanical properties, corrosion behavior and biocompatibility of orthopedic pure titanium−magnesium alloy screw prepared by friction welding [J]. Transactions of Nonferrous Metals Society of China, 2020, 30(11): 2952−2966.

[7] GODFREY T M T, WISBEY A, GOODWIN P S, BAGNALL K, WARD-CLOSE C M. Microstructure and tensile properties of mechanically alloyed Ti−6A1−4V with boron additions [J]. Materials Science and Engineering A, 2000, 282(1/2): 240−250.

[8] KOO M Y, PARK J S, PARK M K, KIM K T, HONG S H. Effect of aspect ratios of in situ formed TiB whiskers on the mechanical properties of TiB_w/Ti−6Al−4V composites [J]. Scripta Materialia, 2012, 66(7): 487−490.

[9] HUANG Li-qing, WANG Li-hua, QIAN Ma, ZOU Jin. High tensile-strength and ductile titanium matrix composites strengthened by TiB nanowires [J]. Scripta Materialia, 2017, 141: 133−137.

[10] HUANG L J, GENG L, PENG H X. In situ (TiB_w+TiC_p)/Ti6Al4V composites with a network reinforcement distribution [J]. Materials Science and Engineering A, 2010, 527(24/25): 6723−6727.

[11] BALAJI V S, KUMARAN S. Densification and microstructural studies of titanium−boron carbide (B_4C) powder mixture during spark plasma sintering [J]. Powder Technology, 2014, 264: 536−540.

[12] ANDO T, NAKASHIMA K, TSUCHIYAMA T, TAKAKI S. Microstructure and mechanical properties of a high nitrogen titanium alloy [J]. Materials Science and Engineering A, 2008, 486(1/2): 228−234.

[13] CONRAD H. Effect of interstitial solutes on the strength and ductility of titanium [J]. Progress in Materials Science, 1981, 26(2−4): 123−403.

[14] ZHANG Y S, ZHAO Y H, ZHANG W, LU J W, HU J J, HUO W T, ZHANG P X. Core-shell structured titanium−nitrogen alloys with high strength, high thermal stability and good plasticity [J]. Scientific Reports, 2017, 7: 40039.

[15] ZHANG Y S, ZHANG W, WANG X, HUO W T. Formation of core−shell network structural titanium−nitrogen alloys with different nitrogen contents [J]. Journal of Materials Science, 2017, 52(13): 7824−7830.

[16] YAZDI R, KASHANI-BOZORG S F. Microstructure and wear of in-situ Ti/(TiN+TiB) hybrid composite layers produced using liquid phase process [J]. Materials Chemistry and Physics, 2015, 152: 147−157.

[17] DAS M, BHATTACHARYA K, DITTRICK S A, MANDAL C, BALLA V K, SAMPATH-KUMAR T S, BANDYOPADHYAY A, MANNA I. In situ synthesized TiB–TiN reinforced Ti6Al4V alloy composite coatings: Microstructure, tribological and in-vitro biocompatibility [J]. Journal of the Mechanical Behavior of Biomedical Materials, 2014, 29: 259−271.

[18] DAS M, BALLA V K, BASU D, MANNA I, SAMPATH-KUMAR T S, BANDYOPADHYAY A. Laser processing of in situ synthesized TiB−TiN-reinforced Ti6Al4V alloy coatings [J]. Scripta Materialia 2012, 66(8): 578−581.

[19] QIU L X, YAO B, DING Z H, ZHENG Y J, JIA X P, ZHENG W T. Characterization of structure and properties of TiN−TiB_2 nano-composite prepared by ball milling and high pressure heat treatment [J]. Journal of Alloys and Compounds, 2008, 456(1/2): 436−440.

[20] BHUIYAN M M H, LI L H, WANG J T, HODGSON P, CHEN Y. Interfacial reactions between titanium and boron nitride nanotubes [J]. Scripta Materialia, 2017, 127: 108−112.
[21] HUANG Li-qing, QIAN Ma, WANG Li-hua, CHEN Zhi-gang, SHI Zhi-ming, NGUYEN V, ZOU Jin. High-tensile-strength and ductile novel Ti−Fe−N−B alloys reinforced with TiB nanowires [J]. Materials Science and Engineering A, 2017, 708(Supplement C): 285−290.
[22] MIN Y, AKBULUT M, KRISTIANSEN K, GOLAN Y, ISRAELACHVILI J. The role of interparticle and external forces in nanoparticle assembly [J]. Nature Materials, 2008, 7: 527−538.
[23] MA Xiao-yan, LI Chang-rong, ZHANG Wei-jing. Study on the phase diagram of the Ti−B−N system and the interfacial reaction of the Ti/BN joints [J]. Materials Science and Engineering A, 2005, 392(1/2): 394−402.
[24] WRIEDT H A, MURRAY J L. The N−Ti (nitrogen−titanium) system [J]. Bulletin of Alloy Phase Diagrams, 1987, 8(4): 378−388.
[25] HUANG L J, GENG L, PENG H X, ZHANG J. Room temperature tensile fracture characteristics of in situ TiB_w/Ti6Al4V composites with a quasi-continuous network architecture [J]. Scripta Materialia, 2011, 64(9): 844−847.
[26] QIAN Ma. Cold compaction and sintering of titanium and its alloys for near-net-shape or preform fabrication [J]. International Journal of Powder Metallurgy, 2010, 46(5): 29−44.
[27] HASHIN Z, SHTRIKMAN S. A variational approach to the theory of the elastic behaviour of multiphase materials [J]. Journal of the Mechanics and Physics of Solids, 1963, 11(2): 127−140.
[28] DOGHRI I, TINEL L. Micromechanical modeling and computation of elasto-plastic materials reinforced with distributed-orientation fibers [J]. International Journal of Plasticity, 2005, 21(10): 1919−1940.
[29] FUKUDA H, KAWATA K. On the stress concentration factor in fibrous composites [J]. Fibre Science and Technology, 1976, 9(3): 189−203.
[30] PENG H X, FAN Z, EVANS J R G. Novel MMC microstructure with tailored distribution of the reinforcing phase [J]. Journal of Microscopy, 2001, 201(2): 333−338.
[31] OVID'KO I A, SHEINERMAN A G. Toughening due to crack deflection in ceramic- and metal-graphene nano-composites [J]. Reviews on Advanced Materials Science, 2015, 43: 52−60.
[32] WANG Y B, WANG L F, JOYCE H J, GAO Q, LIAO X Z, MAI Y W, TAN H H, ZOU J, RINGER S P, GAO H J, JAGADISH C. Super deformability and Young's modulus of GaAs nanowires [J]. Advanced Materials, 2011, 23(11): 1356−1360.
[33] HAN X D, ZHANG Y F, ZHENG K, ZHANG X N, ZHANG Z, HAO Y J, GUO X Y, YUAN J, WANG Z L. Low-temperature in situ large strain plasticity of ceramic SiC nanowires and its atomic-scale mechanism [J]. Nano Letters, 2007, 7(2): 452−457.

网状编织 TiB 纳米线增强具有核壳结构 Ti 基体的高强度 Ti−BN 复合材料

黄立清[1]，黄 群[2]

1. School of Mechanical and Mining Engineering, The University of Queensland, Brisbane, QLD 4072, Australia;
2. 中南大学 粉末冶金国家重点实验室，长沙 410083

摘 要：为提高 Ti 基复合材料(TMCs)的强度，以纳米 BN 粉和 Ti 粉为原材料，采用火花等离子烧结技术制备一种具有新颖结构的 Ti 基复合材料，该复合材料由网状编织结构 TiB 纳米纤维和表面富含 N 溶质原子内部贫 N 的核壳结构 Ti 基体组成。采用 X 射线衍射(XRD)、扫描电子显微镜(SEM)、电子探针显微分析仪(EPMA)和电子万能材料试验机对制备试样的物相组成、形貌、元素分布和力学性能进行测试分析。结果表明，成功制备了具有实验设计特殊结构的 Ti 基复合材料，制备的 Ti−2BN(质量分数，%)复合材料的极限抗压强度达到~1.8 GPa，断裂应变为~9%；Ti−1BN(质量分数，%)的极限抗压强度为~1.6 GPa，断裂应变达到~20%。此外，讨论该复合强化结构在增强 Ti 基复合材料强度中的作用。

关键词：钛基复合材料；TiB 纳米线；氮；网状编织结构；核壳结构

(Edited by Xiang-qun LI)